Temperature modelling in pavements: the effect of long- and short-wave radiation

A. Mammeri[abc], L. Ulmet[a], C. Petit[a] & A.M. Mokhtari[c]

[a] Groupe d'Etude des Matériaux Hétérogènes – Equipe Génie Civil et Durabilité, Université de Limoges, Boulevard Jacques Derche, 19300 Egletons, France

[b] Laboratoire de Mécanique des Structures, Département Génie Civil, BP 417, Université de Béchar, Algeria

[c] Laboratoire Matériaux, Sol et Thermique, Département de Génie Civil, USTOMB, BP 1505 El Menaouer Oran, Algeria
Published online: 15 Jul 2014.

PLEASE SCROLL DOWN FOR ARTICLE

Taylor & Francis
Taylor & Francis Group

Temperature modelling in pavements: the effect of long- and short-wave radiation

A. Mammeri[a,b,c], L. Ulmet[a], C. Petit[a]* and A.M. Mokhtari[c]

[a]*Groupe d'Etude des Matériaux Hétérogènes – Equipe Génie Civil et Durabilité, Université de Limoges, Boulevard Jacques Derche, 19300 Egletons, France;* [b]*Laboratoire de Mécanique des Structures, Département Génie Civil, BP 417, Université de Béchar, Algeria;* [c]*Laboratoire Matériaux, Sol et Thermique, Département de Génie Civil, USTOMB, BP 1505 El Menaouer Oran, Algeria*

This study aims to experimentally validate a 2D finite element model (FEM) in the transient thermal state of a multilayer pavement structure at each given depth. Data model inputs include 15-min values for solar radiation, air temperature and dew temperature, as well as daily values of wind speed obtained from the GEMH-Egletons Laboratory's weather station. This FEM highlights the importance of solar radiation and night-time cooling parameters. A comparison of numerical and experimental results indicates that night-time cooling, despite being often neglected in the literature, is a key parameter for a good surface temperature model, particularly in an arid zone. Also a parameter analysis of this model with various thermal parameters has been made in order to evaluate sensitivity and the main input parameters. The pavement surface is subjected to the strongest temperature variation; hence a good surface temperature assessment provides a key factor for further thermal cracking modelling.

Keywords: thermal modelling; pavement; sky temperature; monitoring; transient

1. Introduction

Pavement cracking constitutes one of the main modes of road degradation. On a multilayer structure, these degradations have a wide array of sources. Traffic and thermal stresses are often at the origin of such damage.

Temporal variations in temperature are especially detrimental to pavements since they induce dimensional variations and cracking due to fatigue (Dempsy *et al.* 1985, Jensen and Hansen 1999). Road design methods in temperate regions around the 45th parallel neglect thermal stress in favour of traffic, yet regions do exist where thermal stresses are indeed dominant (Bissada 1972, Al-Abdul Wahhab and Balghunaim 1994, Abdul Wahhab and Ramadhan 1995), such as in arid zones below the 35th parallel.

Damage occurring in pavements subjected to thermal stresses has not been extensively studied compared with mechanical stresses (Laveissière and Petit 1998). In order to model temperature distribution within the pavement, several studies have been based on either analytical (Lui and Yuan 2000, Tzu-Ping *et al.* 2007, Wang *et al.* 2009) or numerical approaches (Minhoto *et al.* 2006, Jia *et al.* 2007). Other studies have been aimed at characterising surface temperature (Solaimanian and Kennedy 1993), the impact of thermal effects within pavements in a simplified manner (Ramadhan and Al-Abdul Wahhab 1997) or more complete assessments though on shorter sequences (Hermansson 2000, 2004, Yinghong and Hiller 2011).

In a previous study, a thermal finite element model (FEM) using the Cast3M software was developed by considering the solar contribution on the pavement surface. The model spanned one year and concerned a concrete pavement specimen subjected simultaneously to ambient temperature and incident solar flow. The effect of sunshine periods and night-time cooling by radiation towards the sky was taken into account for a dry region, i.e. Béchar in Algeria. The night-time cooling parameter has been proven to be non-insignificant in this region of low cloudiness and moreover can generate a temperature differential in excess of 20 K between day and night.

We are presenting herein an experimental validation of this model using measurements performed on an experimental pavement located at the GEMH-Egletons Laboratory as well as climate data provided by the Egletons Civil Engineering Center's weather station (France). The study period has been appropriately chosen since it is characterised by the near absence of precipitation and clouds, and very strong solar radiation, all of which being similar to dry climate conditions.

The aim of this validation is to show the effectiveness of the night-time cooling effect that is often neglected in the literature and which is taken into account in our numerical model because it is a key parameter for these arid regions. These last are often characterised by a clear sky, and the use of this parameter gives a perfect correlation between simulation and experimental results of the temperature profile on the surface pavement. The obtained results show the performance of the proposed numerical model which contains all the influent parameters which are presented later.

---

*Corresponding author. Email: christophe.petit@unilim.fr

2.   The numerical model

We consider herein a flexible pavement composed of four layers (asphalt concrete (AC), road-based asphalt material (RBA), unbound granular material (UGM) and soil). This structure is subjected simultaneously on its upper surface to convective and radiant exchanges with ambient temperatures and to incident solar flow, whose evolutions are given thanks to local meteorological recordings (see Figure 1).

2.1   *Governing equations*

2.1.1   *Transient conduction*

According to a transient scheme, heat transfer is governed by the following equation:

$$\Delta T = \frac{1}{a}\frac{\partial T}{\partial t}, \tag{1}$$

where T is the temperature (K) defined at time t (s) in the studied volume; Δ is the Laplace operator; a ($= \lambda/\rho C$) is the thermal diffusivity ($m^2\,s^{-1}$), where λ is the thermal conductivity ($W\,m^{-1}\,K^{-1}$), ρ is the density ($kg\,m^{-3}$) and C is the specific heat ($J\,kg^{-1}\,K^{-1}$). The values of λ, C and ρ are defined in Section 4.3.

2.1.2   *Convection*

Convection refers to the heat transfer process between the pavement surface and the surrounding air. The density of convective flux ϕ_{conv} ($W\,m^{-2}$) is given by Newton's Law:

$$\phi_{conv} = h(T_s - T_{air}), \tag{2}$$

where T_s is the surface temperature (K) and T_{air} is the air temperature (K). h is the convection heat transfer coefficient ($W\,m^{-2}\,K^{-1}$). An analysis of air velocities

Figure 1.   Flows exchanged on the pavement.

recorded in the climate data file leads to consider the forced convection condition during the modelled period. The formula used in this study is given by (Yinghong and Hiller 2011)

$$h = 5.6 + 0.332 Re^{0.5}Pr^{1/3}\frac{K_{air}}{L}, \tag{3}$$

where for air $K_{air} = 0.027$, $Pr = 0.7$, and, considering the surface pavement as an infinite plate, $L = 0.15\,m$. The Reynolds number is

$$Re = \frac{VL}{\nu}, \tag{4}$$

where V is the local wind velocity ($m\,s^{-1}$) and $\nu = 16.01 \times 10^{-6}\,m^2\,s^{-1}$ is the air kinematic viscosity.

2.1.3   *Radiation*

Two types of radiant exchanges coexist at the surface of the slab:

- Solar irradiation transmits energy onto the pavement surface as a short wavelength (SWL). The reflected portion of the incident short-wave radiation is given by the albedo coefficient of the pavement surface. The remaining portion is absorbed by the slab, which causes the surface temperature to rise. The absorption coefficient ratio depends on the colour of the AC, which may be weathering dependent.
- Radiation towards the sky is of the long wavelength (LWL) type and follows the Stefan–Boltzmann law, i.e.

$$\phi_{LWL} = \varepsilon\sigma(T_s^4 - T_{sky}^4), \tag{5}$$

where ε is the emissivity of the pavement surface, σ is the Stefan–Boltzmann constant (5.67×10^{-8} $W\,m^{-2}\,K^{-4}$) and T_{sky} is the equivalent temperature of radiation of the sky (K). Among the various available expressions of T_{sky} found in the literature, we focus on the three following:

- First expression: $T_{sky\,0}$
  In this simplest expression, the temperature of radiation of the sky is identical to the air temperature. This enables to use a global superficial exchange coefficient, including both radiation and convection.

$$T_{sky\,0} = T_{air}. \tag{6}$$

- Second expression: $T_{sky\,1}$
  The LWL radiation towards the sky depends on the absorption by water molecules present in the

surrounding atmosphere. According to this point, the sky temperature expression is calculated based on air temperature T_{air} (K) and sky emissivity ε_0 (Yinghong and Hiller 2011):

$$T_{sky\,1} = \varepsilon_0^{0.25} \times T_{air}, \tag{7}$$

where ε_0 depends on the local dew point temperature θ_{dp} (°C) as follows:

$$\varepsilon_0 = 0.754 + 0.0044\theta_{dp}. \tag{8}$$

- Third expression: $T_{sky\,2}$
  The sky emissivity is also shown to be cloud-covering dependent. This influence is usually included in building dynamic thermal simulations, and this article suggests introducing it in pavement modelling. The chosen formula is that used in the TRNSYS software (Martin and Berdahl 1984):

$$T_{sky\,2} = T_{air}(\varepsilon_0 + 0.8(1 - \varepsilon_0)C_{Cover})^{0.25}, \tag{9}$$

where ε_0 represents the emissivity of a clear sky; it is calculated as a function of the local air dew point temperature θ_{dp} (°C):

$$\varepsilon_0 = 0.711 + 0.0056\theta_{dp} + 7.3 \times 10^{-5}\theta_{dp}^2$$
$$+ 0.013\cos\left(2\pi\frac{hour}{24}\right) + 1.2$$
$$\times 10^{-4}(p_{atm} - p_0), \tag{10}$$

and additional corrections where *hour* is the hour of the day, in solar time; p_{atm} and p_0 denote the local atmospheric pressure (hPa) and atmospheric pressure at sea level ($p_0 = 1013.25$ hPa), respectively.

p_{atm} is approximated by

$$p_{atm} = p_0\,e^{\rho_0 h/p_0}, \tag{11}$$

where g is the gravity acceleration (9.81 m s^{-2}), h is the altitude above sea level (m) and ρ_0 is the air density at sea level (1.225 kg m^{-3}).

C_{cover} represents the cloud layer factor. If there are no data available, this parameter can be determined according to the following equation:

$$C_{Cover} = \left(1.4286\frac{E_{Dif}}{E_{Glob,H}} - 0.3\right)^{0.5} \tag{12}$$

with E_{Dif} the diffuse flow and $E_{Glob,H}$ the total flow of radiation at a horizontal surface. If diffuse flow is not directly measured, it can be estimated from a comparison between the effective value of the total flow and its theoretical value under clear sky conditions. For the night period, the cloud layer factor is assumed to be an extrapolation of the average value over the preceding afternoon.

2.2 Finite element modelling

The numeric model is based on a finite element method using the Cast3M software. The input data are thickness of the layers, material properties and effective evolutions of climatic parameters (i.e. temperature and humidity of ambient air, solar radiation, sky temperature, wind speed). The outputs are the profiles of temperature fields along the depth of the slab ant its soil sub-base. Some evolutions are computed at particular depths corresponding to sensors positions, in order to be compared with the measure.

2.2.1 An overview of Cast3M

Cast3M is a finite element method environment, initiated in the Department of Mechanics and Technology (DMT) of the French Atomic Energy Commission (www-cast3m.cea.fr). The development of Cast3M is part of the activity of research in the field of mechanics, the aim being to establish a high-level instrument that can serve as valuable support for the conception, design and analysis of structures and components, in the nuclear field as in the classical industry. This free and open-source software is widely distributed in universities or research centres, and is continuously incremented thanks to these partner's scientific works, under the supervision of the DMT. Cast3M presents a complete system, including not only the calculation functions themselves, but also functions to build the model (pre-processor) and treatment outcomes (post-processor). Unlike other classical codes, which can be seen like 'black boxes', Cast3M enables the user to build his own treatment by binding some elementary processes. Reaching this flexibility requires mastering a specific language 'GIBIANE', which presents all the characteristics of an object-oriented programming language.

In this context, Cast3M can solve a wide range of problems, such as linear elasticity in statics and dynamics steady-state or transient thermal diffusion, nonlinearities in mechanics (elasto-viscoplasticity, damage), fracture mechanics, contacts and fluid flow. Any coupling between these various domains can also be carried out.

2.2.2 Principle of FEM transient heat transfer modelling

The discretisation of a transient heat transfer problem classically leads to the following system:

$$\underline{\underline{C}}.\dot{\underline{T}} + \underline{\underline{K}}.\underline{T} = \underline{Q}, \tag{13}$$

where $\underline{T}$ is the vector of nodal temperatures, and $\underline{\dot{T}}$ the vector of their time derivatives, $\underline{\underline{C}}$ is the capacity matrix, which depends on specific heat and density of the materials, $\underline{\underline{K}}$ is the conductivity matrix, which depends on thermal conductivity of the materials and $\underline{Q}$ is the thermal loading vector, function of limit conditions applied along the boundaries of the domain: external flows, imposed temperatures, convective or radiant boundary conditions.

The transient FEM algorithms developed in the Cast3M environment are based on an incremental scheme (called 'Theta Method'), designed as nonlinear in order to take, for example, the radiation equation into account.

This method consists of translating Equation (13) into the following family of relations, depending on the θ parameter as

$$\frac{1}{\Delta t}\underline{\underline{C}}^*.(\underline{T}^{n+1} - \underline{T}^n) + \underline{\underline{K}}^*(\theta\underline{T}^{n+1} - (1 - \theta)\underline{T}^n) = \underline{Q}^*, \quad (14)$$

where $\underline{T}^{n+1}$ is the temperature vector at the time step $n + 1$, $\underline{T}^n$ is the temperature vector at the time step n, Δt is the time step and θ is the relaxation coefficient, $(0 \le \theta \le 1)$, which enables a choice among various transient schemes: explicit ($\theta = 0$), full-implicit ($\theta = 1$) or Crank–Nicolson ($\theta = 1/2$). Intermediate values for θ can also be chosen. The stability of the scheme depends on the choice of θ: unconditional if $\theta \ge 1/2$, or subject to a maximum value of time step if $\theta < 1/2$.

The superscript * means that the matrices and the second member are evaluated, at the temperature $T^* = bT^{n+1} + (1 - b)T^n$, or at the time $t^* = bt^{n+1} + (1 - b)t^n$, respectively, b being the coefficient of sub-relaxation ($0 \le b \le 1$).

In order to ensure the convergence, we have chosen the following parameters: $\theta = 1$ and $b = 1$.

The construction of the thermal loading vector (second member) is carried out at each time step and depends on predefined evolutions of climatic or exchange conditions. Air and sky temperatures and solar radiation scenarios are actually known, as well as convection coefficient, which may depend on wind speed.

Concerning the boundary condition of radiation type, factoring $T_s^4 - T_{sky}^4$ as follows:

$$T_s^4 - T_{sky}^4 = (T_s - T_{sky})(T_{sky}^3 + T_{sky}^2 T_s + T_{sky} T_s^2 + T_s^3). \quad (15)$$

It enables to treat this condition as a convection type:

$$\phi_{LWL} = \varepsilon\sigma(T_{sky}^3 + T_{sky}^2 T_s + T_{sky} T_s^2 + T_s^3)(T_s - T_{sky})$$

$$= h_r(T_s - T_{sky}), \quad (16)$$

where h_r depends on the effective surface temperature.

The Cast3M procedure called 'PASAPAS' executes a step-by-step calculation of the evolution of the temperature field from a known initial state. For non-linear laws such as radiation, an internal loop works at each time step until convergence is reached. Once input parameters are conveniently defined, this process is user transparent.

2.2.3 *Pavement finite element modelling*

The edge effects induced by the road shoulders are supposed to be negligible, so that the pavement area can be considered as infinite. The diffusion problem is therefore of 1D-type. However, the numerical model is chosen bidimensional, considering that Cast3M meshing options are restricted to 2D or 3D. The mesh is composed of a stacking of 61 single eight-noded quadrilaterals ('QUA8' Cast3M-type with quadratic interpolation), in order to spare computation time (see Figure 2). Different material properties are assigned to the elements belonging to the respective layers of the pavement. The soil is extended to a depth of 20 m with elements of progressive size. An adiabatic boundary condition is imposed at the bottom of the soil, and computations have shown that the annual variation of temperature becomes negligible at this depth. This option avoids the choice of an arbitrary and generally unrecognised temperature in deep soil, as required by others models such as EICM. Let us note that the geothermal gradient has been here neglected.

The initial temperature field in the instrumented part of the slab is provided by linear interpolation between the data given by the sensors at a starting instant. However, we have no access to the initial temperature distribution in the deep soil. It is estimated by an analytic way, considering the soil as a semi-infinite domain of which the surface is at the T5 sensor level. The limited condition applied on the boundary is an imposed yearly sinusoidal temperature evolution, which is identified to match the T5 recordings. However, the initial profile in deep soil has been shown to have a weak influence on the pavement's temperature. Then, a few-day simulation is necessary in order to make sure that the approximation introduced by linear interpolation on initial values will vanish. The effective computation aiming to compare with the experimental recordings can afterwards be carried-out.

The necessary data to compute the variable boundary conditions applied to the surface are provided by ASCII files generated by the meteorological acquisition devices. These are as follows:

- air temperature;
- global solar flow incident on an horizontal surface;
- sky radiant temperature (pre-computed by a specific software, depending on air temperature, relative humidity and solar flow recordings) and
- wind speed (in order to compute the convection exchange coefficient).

The introduction in Cast3M of the evolution of these data sequenced every 15 min enables to compute the second member Q^* at each time step.
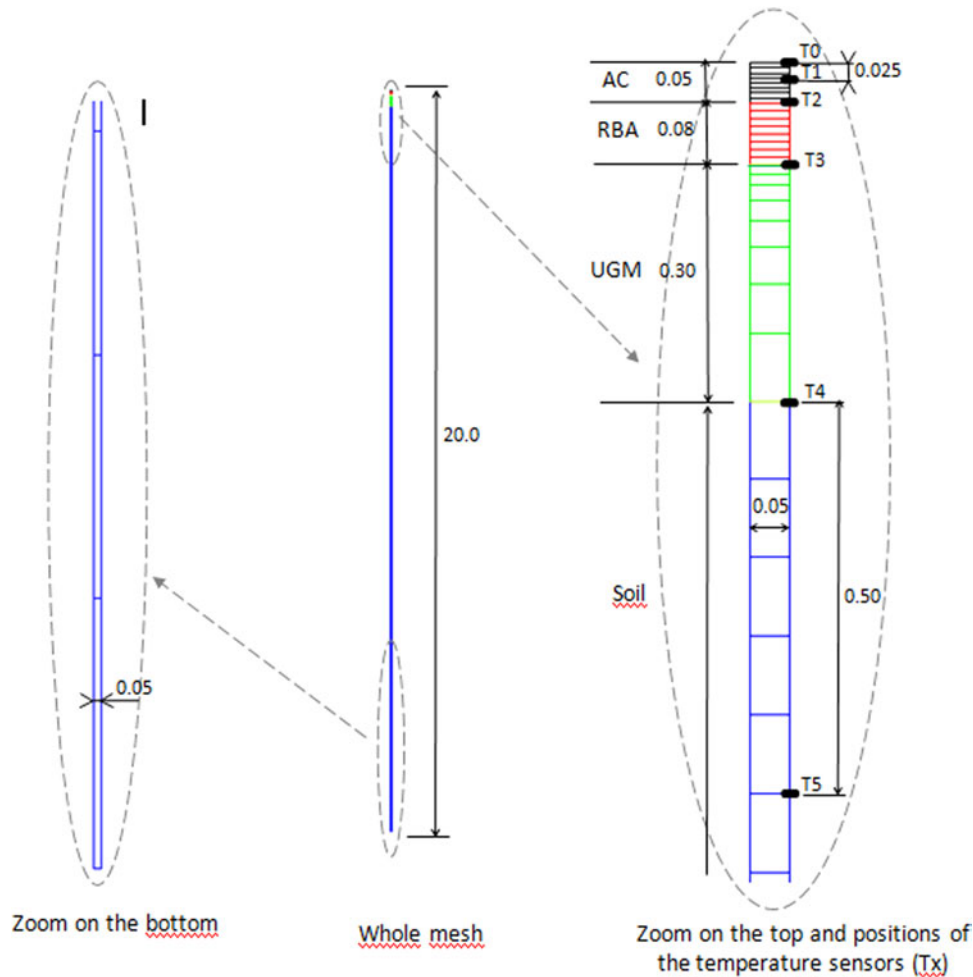
Figure 2. FEM mesh and position of thermal sensors in the pavement.

The results of finite element calculations pertain to temperature evolution at particular depths in the pavement structure, i.e. depths that coincide with sensor locations (T0, T1, T2, T3, T4 and T5) (Figure 2). The ultimate aim is to compare experimental recordings with numerical trends, in order to prove the efficiency of this model for an annual simulation.

3. Experimental campaign

The proposed case study corresponds to an experimental pavement set-up at the GEMH Laboratory in Egletons (University of Limoges, France). Initiated in March 2007, this 70 m × 10 m pavement was laid to both study the diagnostic methods for flexible pavements and monitor their evolution over time. The set-up features three different types of structures including the one modelled herein (Figure 2), which consists of a conventional structure intended for medium traffic and composed of a ground support, a 30 cm layer of UGM, a 8 cm layer of RBA and a 5 cm layer of AC (El Ayadi *et al.* 2012). The

material used as surface layer is a French standard HMA BBSG [NF P98-130], with a formulation 0/10. It contains gravel 0/2, 2/6 and 6/10, where the contribution of limestone fine was also used. The binder utilised is traditional asphalt with pen 35/50 with a content of 5.7% by weight of mix.

During its construction, this structure was instrumented with a surface sensor (T0), one sensor on each interface (T2, T3 and T4), an intermediate sensor in the AC layer (T1) and an in-depth sensor placed in the ground (T5; Figures 2 and 3).

Figure 4 shows the set of instruments of the GEMH-Egletons Laboratory's weather station, which is used to obtain the external boundary conditions as data for the FEM. The *in situ* meteorological variables are air temperature and relative humidity (both given from a thermo-hygrometer sensor), total incident solar radiation on a horizontal surface and wind speed. As the pavement is horizontal, the measured solar radiation can be straightforwardly applied, without any incidence correction formula.

Figure 3.   Layout of the temperature sensors.

Figure 4.   Weather station serving the university campus.

The experimental campaign presented in this article extends over 1 year (from July 2012 to July 2013). The experimental acquisition is completed every 15 min, as well for climatic recordings, as for pavement temperature recordings.

4.   Results and discussion

The aim of this section is to validate a thermal modelling which will be coupled in future with a mechanical model for predicting thermal fatigue damage and cracking. Therefore, we remind that the objective of this article is to evaluate the daily temperature variation in the pavement with the key parameters from weather data. The greatest variation occurs at the pavement surface and close to the surface. Therefore, in this article, we focus first on the surface temperature modelling which greatly depends on environmental parameters and surface thermal properties. Second, we look at inside temperature which mainly depends on thermal asphalt material properties.

Section 4.2 proposes to study the main and sensitive environmental parameters such as sky temperature modelling, and wind modelling. The surface properties are also identified. For this study, we focus on five days from 25 to 29 July 2012. This period is opportunely chosen for its contrasted feature: the first three days end a sequence of many identical days characterised by dry, cloudless and sunny conditions. Afterwards, a stormy degradation occurs from the dawn of the fourth day. Wind is also varying from calm (0 km/h) to 2 km/h

(see Figure 5). Then, short-term modelling with various sky and wind conditions can be done.

After validation of surface temperature modelling, we look at temperature inside asphalt layers on only two days because the environmental parameters are no longer the main parameters, we can then focus on thermal conductivity and thermal inertia sensitivity.

The future objective is to use this model over one or several years, in order to simulate thermal damage; therefore, in Section 4.4, we propose a statistical analysis of the surface temperature numerical response compared with experimental temperature data. This section enables us to identify whether the model is always adapted in all weather conditions and what kind of weather needs improvements. We can also run statistical analysis with more than 200 data (more than 6 months) with a lot of daily temperature variation simulation to compare with experimental measurements. Conclusion can then be done for predicting mechanical thermal stresses induced in the concrete pavement for predicting cracking and damage.

4.1   *Parameters reference values*

Reference values are set for the surface and materials parameters (see Table 1). Each of them is justified in the later sections. Sensitivity to these parameters is shown as well.

4.2   *Environmental and surface parameters: effect on surface temperature*

Figure 6 presents the balance of the various flows exchanged on the surface pavement for the selected 5-day sequence. These are absorbed solar irradiation, LWL radiation towards the sky, convection with air and conduction from the slab. They are estimated from the measured surface temperature recordings. Notice that these respective flows are characterised by comparable amounts, so that none of them can be neglected or evaluated with poor accuracy.

4.2.1   *Sky temperature modelling*

In order to illustrate the respective features of the three T_{sky} formulas, regardless of others phenomena, another short period has to be chosen (18–21 July 2012) because it
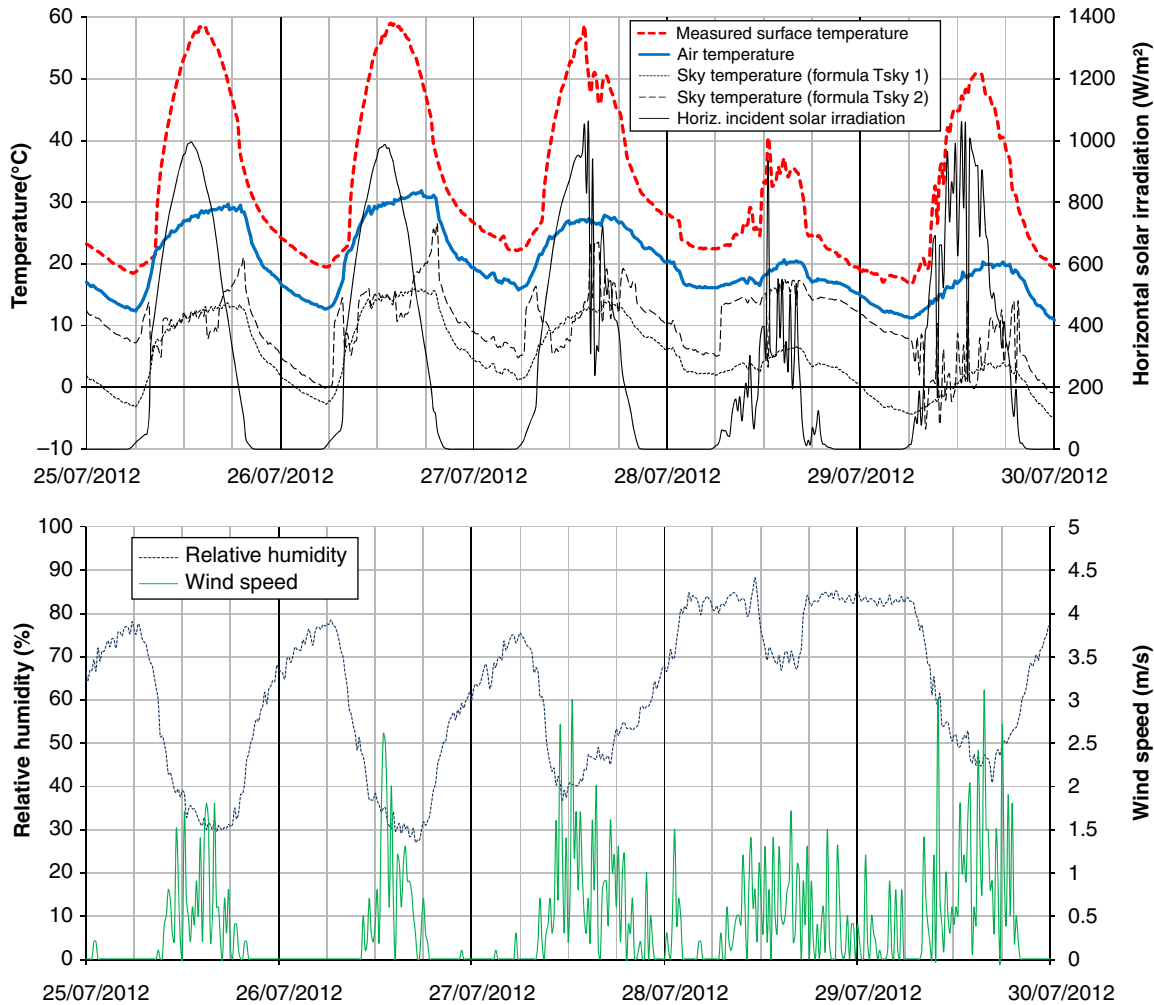
Figure 5. Example of climatic recordings and computed sky temperatures for 5 days.

is characterised by variable sky coverings, but no rain. Figure 7 shows the evolutions of the surface temperatures computed with the three T_{sky} formulas, compared with the experimental data. These three curves can be related to

Table 1. Default values of thermal properties used in the model.

Material properties			
Layers	λ (W m^{-1} K^{-1})	C (J kg^{-1} K^{-1})	ρ (kg m^{-3})
AC	1.63	712	2530
RBA	1.63	712	2530
UGM	1.8	964	2200
Soil	1.1	840	1299
Surface properties			
Emissivity, ε	Absorption coefficient, $a = 1 -$ Albedo		Convection heat transfer coefficient (W m^{-2} K^{-1})
0.93	0.90		Wind speed dependent

their respective T_{sky} evolutions. The choice of $T_{sky\,0}$ systematically overvalues the surface temperature of $2-5$ K. However, using $T_{sky\,1}$ and $T_{sky\,2}$ leads to a very good accuracy for a cloudless day (18th July). Notice that these two formulas give comparable T_{sky} values for a sky clear. A gap between these occurs when the sky is overcast (20th July). Then, $T_{sky\,2}$, which takes the cloud layer factor into account, is logically close to the air temperature than $T_{sky\,1}$. Whatever the climatic conditions are, the best fit with the experimental curve is obtained for $T_{sky\,2}$ formula, especially at the daily minimum which occurs at sunrise.

Many researchers (Minhoto *et al.* 2006, Hermansson 2004, Hall *et al.* 2012) have chosen the use of air temperature as external body temperature for the radiation effect. As shown in this section, this hypothesis leads to significant differences in temperature measurements especially when the sky is clear. Using a simple correlation formula such as $T_{sky\,1}$ may be sufficient only for arid areas, but not for oceanic areas which are subjected to variable cloud coverings.
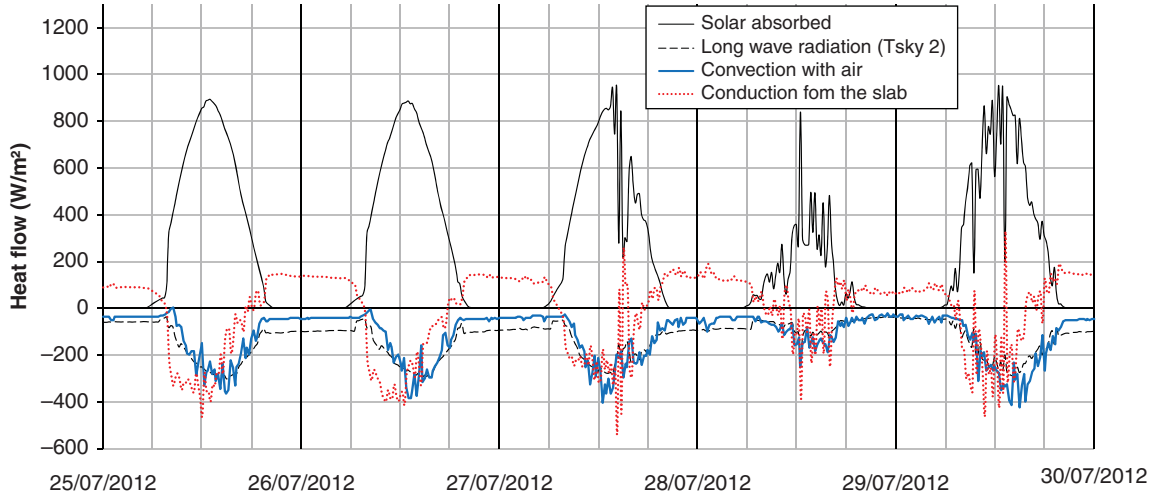
Figure 6.   Energy balance of the surface pavement.
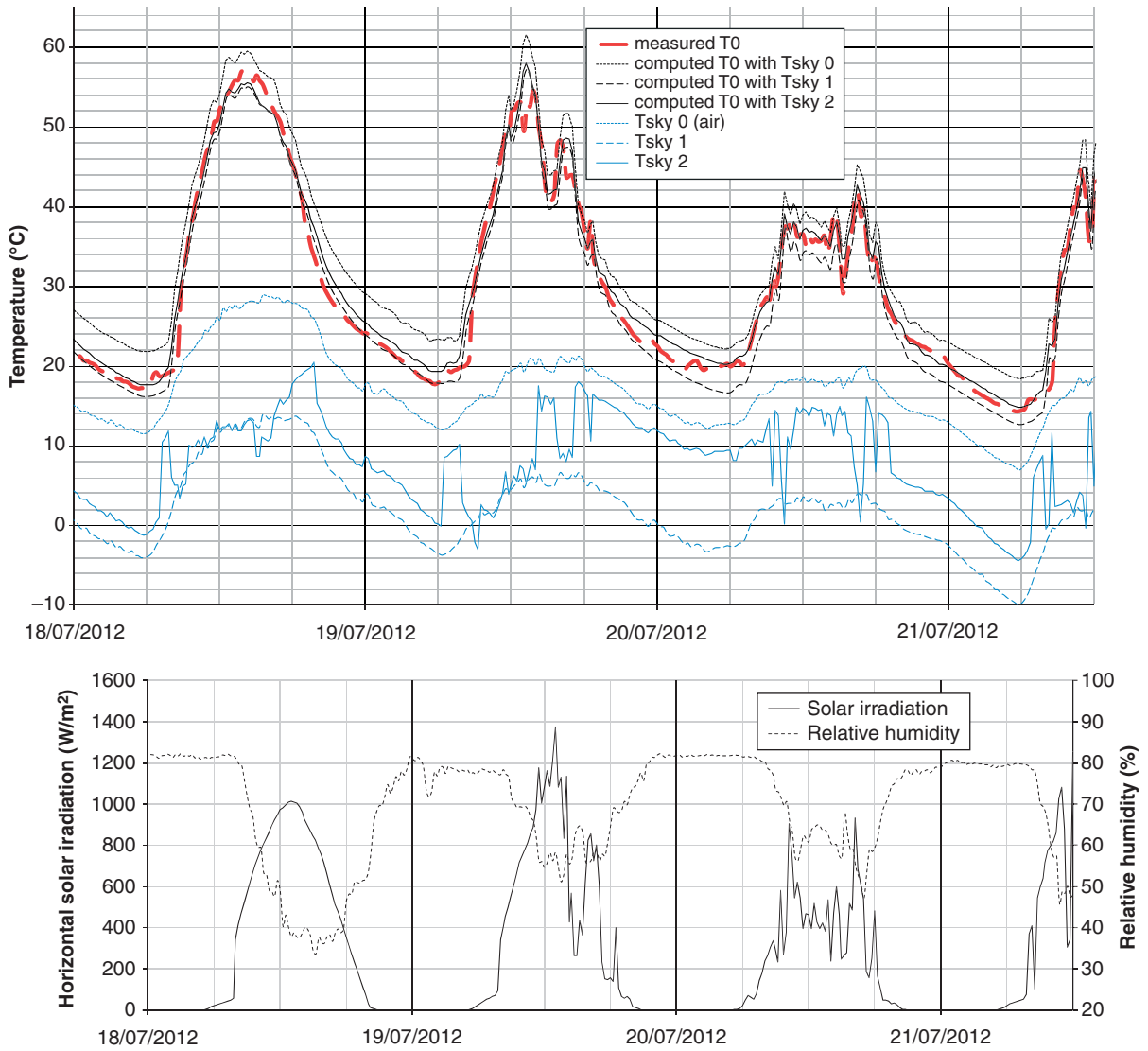
Figure 7.   Influence of the choice of T_{sky} formula on the accuracy of surface temperature T0.
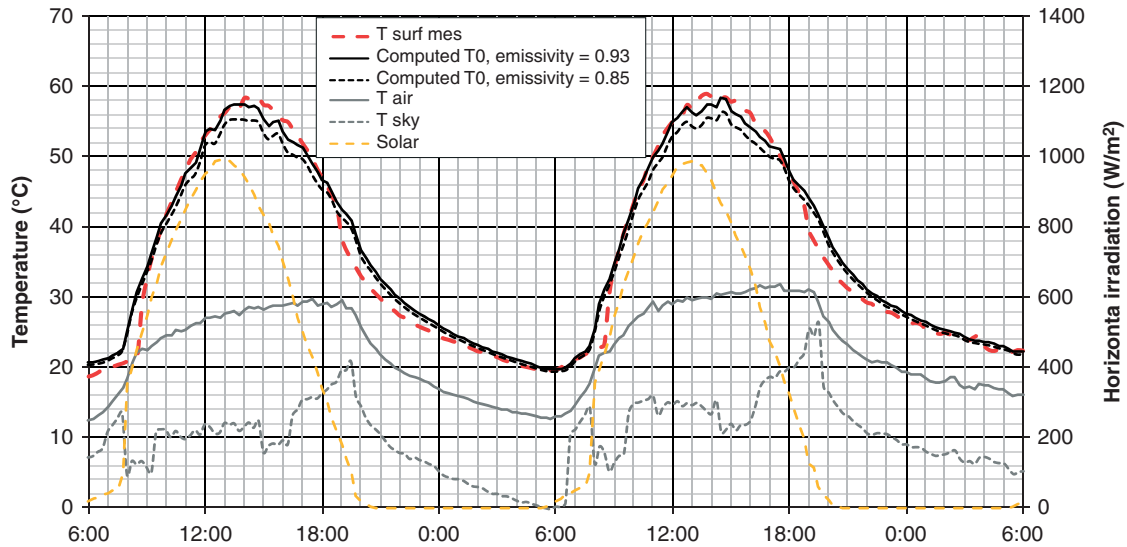
Figure 8. Influence of the emissivity on the computed surface temperature T0 (25–26 July 2012).

As reported by other authors (Hall *et al.* 2012, Tao and Shide 2012), we have incorporated cloud conditions effectively. It points out the benefit of using a precise and well-tested correlation formula issued from the thermal simulation of buildings. Following this validation, we selected the numerical model based on the $T_{sky\,2}$ principle for the remainder of this study.

4.2.2 Surface parameters

In this section, we are interested in the sensitivity of surface parameters such as emissivity ε and solar

absorptivity α coefficients. The data encountered in the literature show that the range of variability of the emissivity of AC surface is limited from 0.85 (Hermansson 2004) to 0.93 (Tzu-Ping *et al.* 2007). A value of 0.9 is frequently used (Minhoto *et al.* 2006, Yinghong and Hiller 2011). In Figure 8, we can identify the small effect of emissivity coefficient; the maximum effect, about 2 K, occurs at the peak. Our default value of surface emissivity is set to 0.93. In general, absorptivity of materials may strongly depend on the wavelength range of the radiation: SWL as solar radiation, or LWL as emission of terrestrial bodies. SWL absorptivity is directly related to the colour
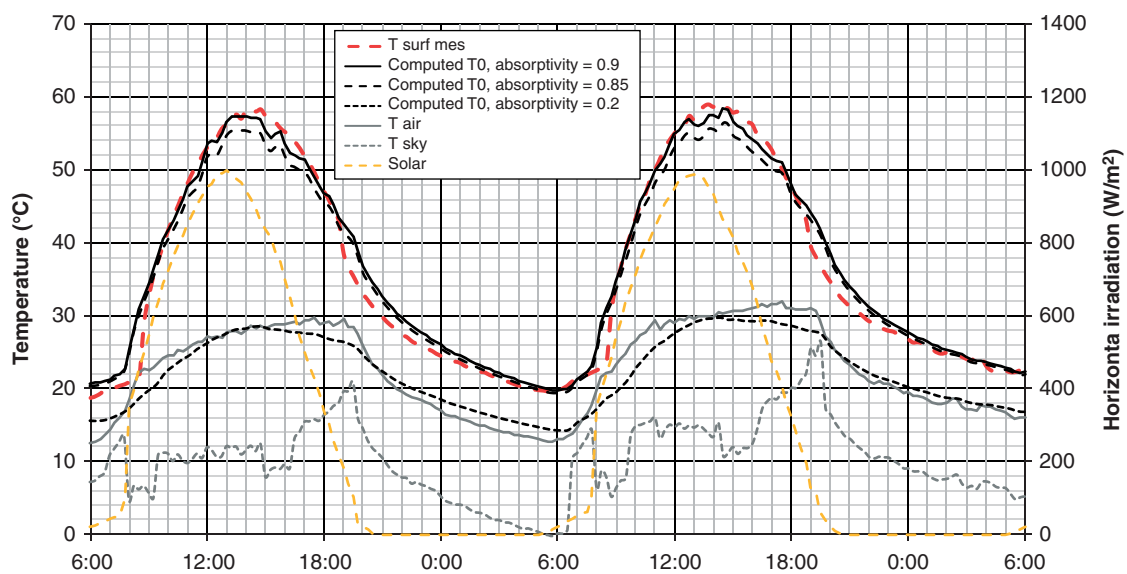
Figure 9. Influence of the absorptivity on the computed surface temperature T0 (25–26 July 2012).
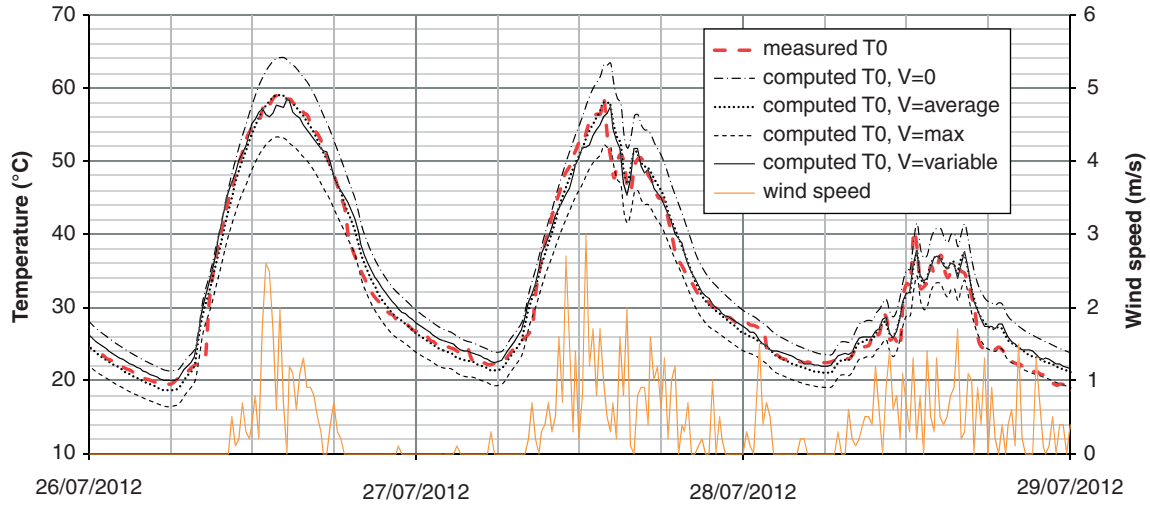
Figure 10.   Influence of the selected wind speed for convection on the computed surface temperature T0.

(light or dark) of the surface. The absorptivity of AC surface taken into account in our model equals 0.90 (Marcel *et al.* 2003). This corresponds to a new surface pavement, for which aggregates are asphalt-covered, which is the case of the tested slab. Absorptivity of the AC after traffic and environment ageing depends on the type of aggregates used, the colour and the texture of the mix and probably some other factors. To show the impact of this coefficient, a value $\alpha = 0.85$ (old surface pavement) was selected for short-term sensitivity analysis (see Figure 9). As for emissivity, this parameter in its usual range of variation has slight effect on the surface

temperature. In addition, Figure 9 points out the strong impact of light coverings as white painting for markings ($\alpha = 0.2$). These can generate strong contrasts in the temperature fields between painted parts of the pavement (i.e. stripes, arrows) and the unpainted parts. This can explain the frequent cracks occurring in the vicinity of boundaries between painted and bare surfaces.

4.2.3   Wind parameters

This section details the sensitivity of wind velocity by the way of convection heat transfer coefficient in the
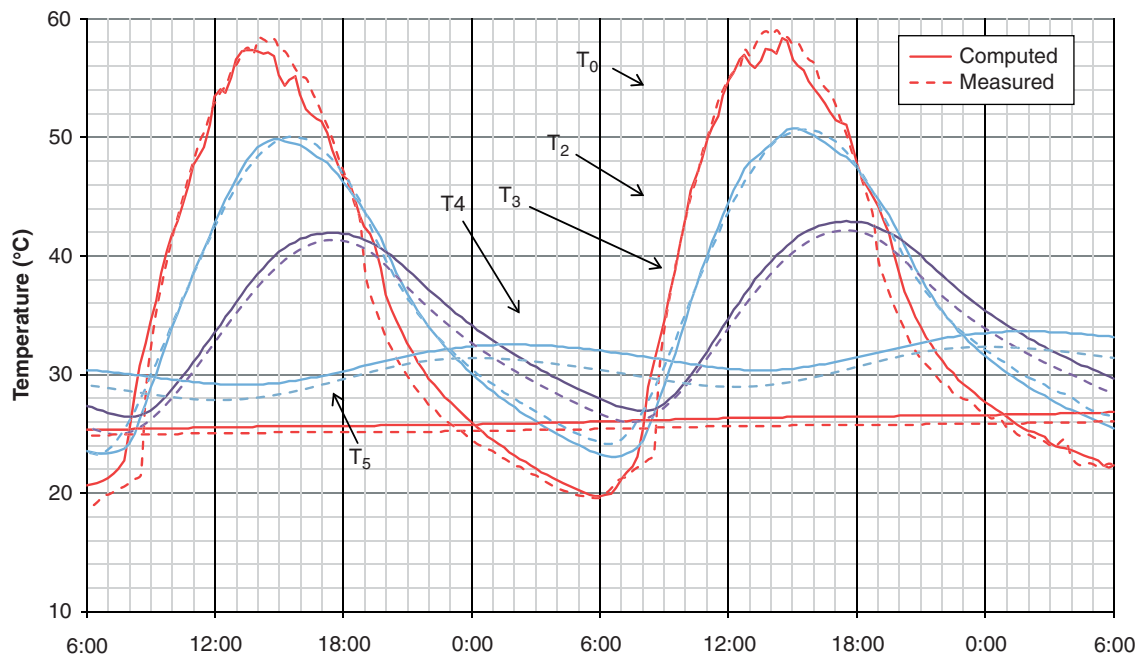
Figure 11.   Temperature evolutions at sensor positions (26 July 2012).
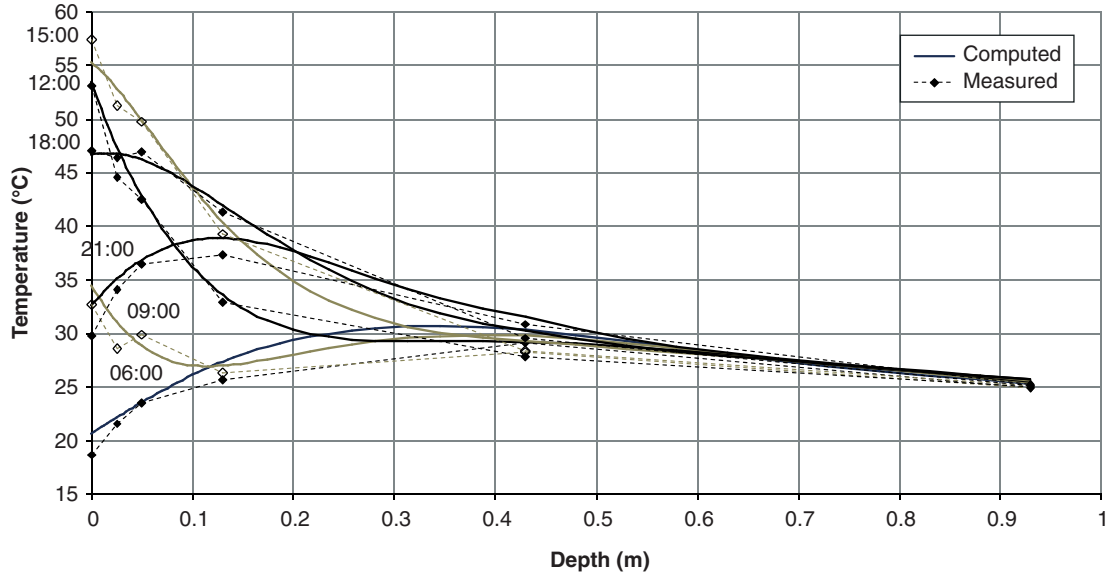
Figure 12. Temperature profiles in the slab at various instants (26 July 2012).

thermal modelling. It is calculated using the formula (3) with different values of wind speed encountered during the studied period: $V_{min} = 0$ m/s, $V_{average} = 0.38$ m/s, $V_{max} = 3.1$ m/s and V variable, which give the following coefficients, respectively: $h = 5.6$ W m^{-2} K^{-1}, $h = 8.8$ W m^{-2} K^{-1}, $h = 14.6$ W m^{-2} K^{-1} and h variable according to Equation (3). In Figure 10, we observe that this parameter has a significant impact on the correct estimation of the profile of surface temperature, which perfectly coincides with experimental results at peak, when the value of h is variable. This section shows that

wind is very important for a good prediction of surface temperature.

4.3 *Thermal pavement material parameters: effect on inside pavement temperature*

This section deals with the analysis of sensitivity of internal temperature profiles to material thermal properties input data: thermal conductivity λ and heat storage capacity $\rho \times C$. As density ρ and specific heat C play the same role in the product $\rho \times C$ encountered
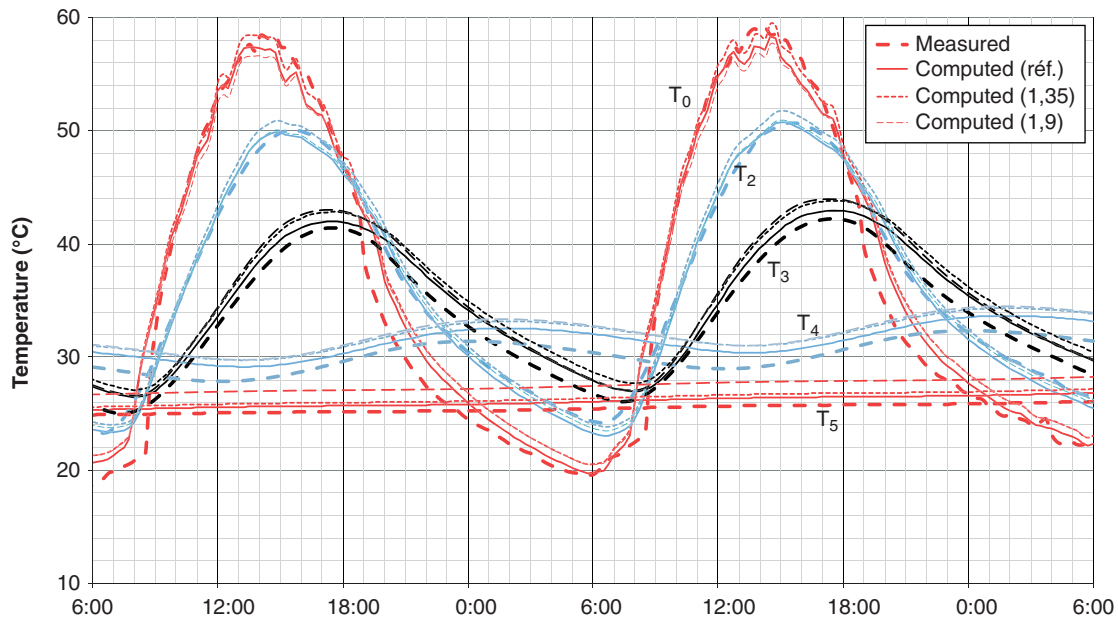
Figure 13. Influence of thermal conductivity (AC + RBA).

Table 2. Sensitivity of computed extreme temperatures towards the input material parameters for a clear day (26 July 2012).

			AC and RBA				UGM			
			Influence of conductivity (ref: $\lambda = 1.63\,W\,m^{-1}\,K^{-1}$)		Influence of specific heat (ref: $C = 712\,J\,kg^{-1}\,K^{-1}$)		Influence of conductivity (ref: $\lambda = 1.8\,W\,m^{-1}\,K^{-1}$)		Influence of specific heat (ref: $C = 964\,J\,kg^{-1}\,K^{-1}$)	
Sensor position	Measured (°C)	Computed (°C) (with refer. data)	$\lambda = 1.35$	$\lambda = 1.9$	$C = 640$	$C = 783$	$\lambda = 1.44$	$\lambda = 2.16$	$C = 1500$	$C = 500$
T0 (surface)										
Max. (°C)	59.1	58.3	59.5	57.7	58.8	57.9	58.6	58.4	58.0	58.7
Min. (°C)	19.6	19.8	20.5	20.5	19.4	20.1	19.8	20.0	19.8	19.6
Ampl. (K)	39.5	38.6	39.0	37.2	39.4	37.8	38.8	38.4	38.2	39.1
T3 (RBA/UGM)										
Max. (°C)	42.2	42.9	43.8	44.0	43.2	42.7	43.8	42.6	41.5	44.8
Min. (°C)	26.1	27.0	27.7	27.0	26.7	27.2	26.8	27.5	27.4	26.0
Ampl. (K)	16.2	16.0	16.1	17.0	16.5	15.4	17.0	15.1	14.1	18.8
T4 (UGM/soil)										
Max. (°C)	32.4	33.5	34.2	34.4	33.6	33.5	33.2	34.6	32.1	35.3
Min. (°C)	29.0	30.4	31.0	31.0	30.3	30.4	30.8	31.0	30.4	29.8
Ampl. (K)	3.4	3.1	3.2	3.4	3.3	3.0	2.5	3.7	1.7	5.5
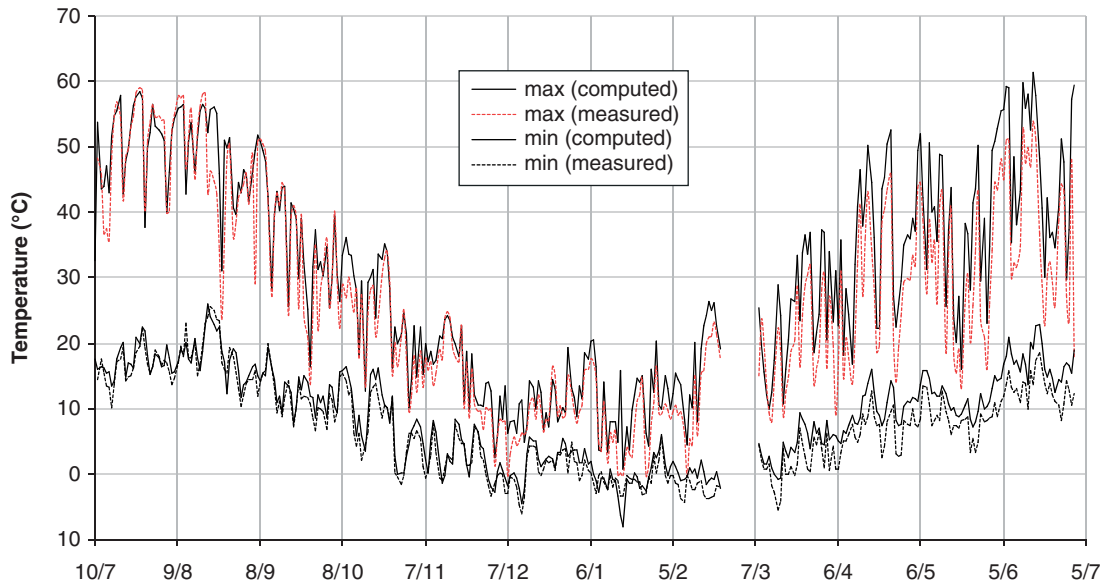
Figure 14. One-year surface temperature simulation (2012–2013): extreme daily temperatures.

in the set of equations, the sensitivity study will only concern *C*.

Concerning the AC, the chosen default values (see Table 1) are issued from Nguyen Q.T. (Nguyen 2011, Nguyen *et al.* 2012), who carried out laboratory tests by an FP2C device technique. This provides the determination of conductivity and specific heat at the same time. For this normalised AC, bitumen and aggregates are the same in

laboratory as in the field on pavement section test used in this study. Bitumen is also 35/50 Pen and content 5.7% of aggregate. Aggregate grading curve and origin (quarry) are the same. The properties of the UGM are given in Vautrin and Livet (1996).

Figure 11 compares the numerical and experimental evolutions during two sunny days, at various depths of the pavement structure. This comparison is also illustrated in
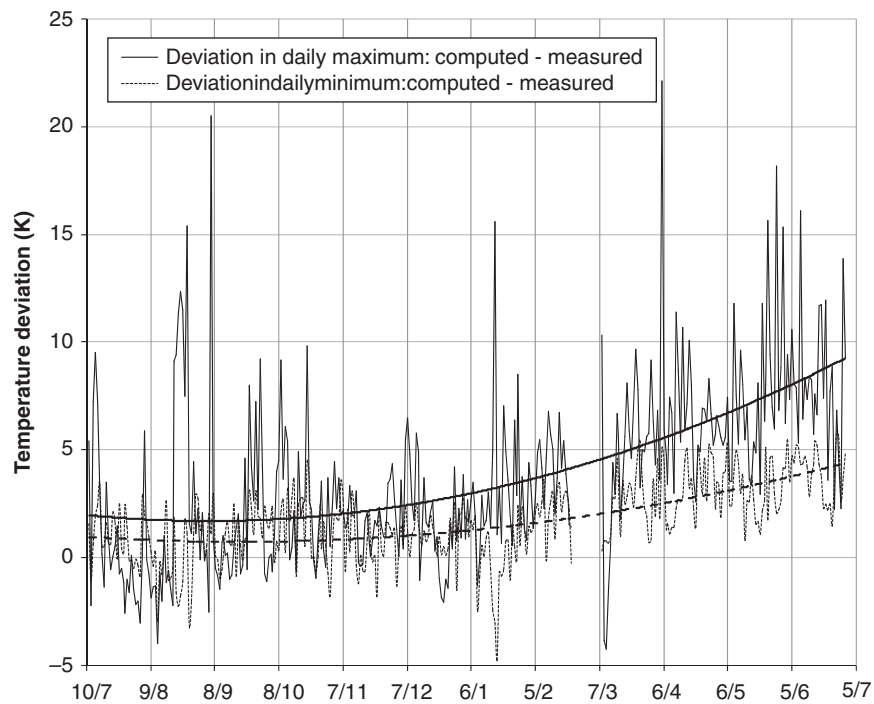
Figure 15. Temperature deviation of the model (1-year modelling).
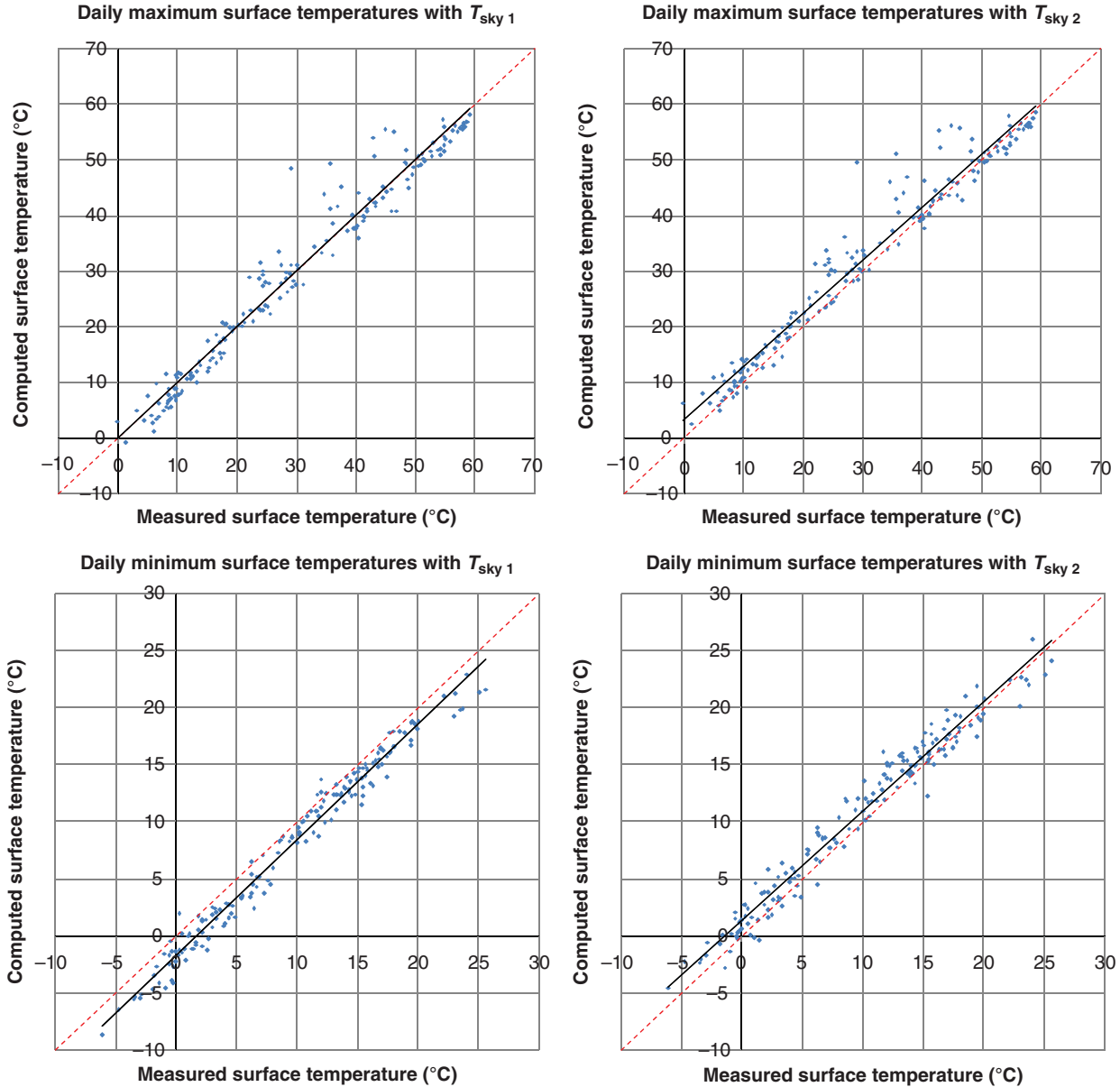
Figure 16. Daily peak and valley surface temperatures, numerical versus experimental comparison (10 July 2012 to 31 December 2012).

terms of temperature profiles in the slab (Figure 12). It can be noted that the two results lie close together, especially in the AC and RBA layers, thus demonstrating that the model's results issued from laboratory-determined thermal properties yield an excellent temperature prediction. However, a small variation in amortisation or phase shift is also noticed at the bottom of the UGM layer, due to the variability of thermal properties in this kind of material.

In Figure 13, we can see that the numerical results with various values of thermal conductivity of AC and RBA in the range $1.35-1.9\,\mathrm{W\,m^{-1}\,K^{-1}}$ are slightly sensitive to this parameter. As for the conductivity, the influence of thermal inertia cannot be pointed out very clearly in a

graphic form. Table 2 sums up the sensitivity study by reporting daily maxima, minima and amplitudes of surface and interface temperatures, only.

If we consider the daily temperature amplitude as the main source of damage, this sensitivity study shows that the accuracy of material properties inputs is not much critical for a good assessment of the lifetime of a pavement. The variation of conductivity or inertia parameters in a realistic range for AC and RBA does not impact the amplitude over 1 K for the structural layers of the slab. In the same manner, UGM which may present a greater variability of properties (depending on quarry and water content) is shown to have only a slight influence on upper layers.
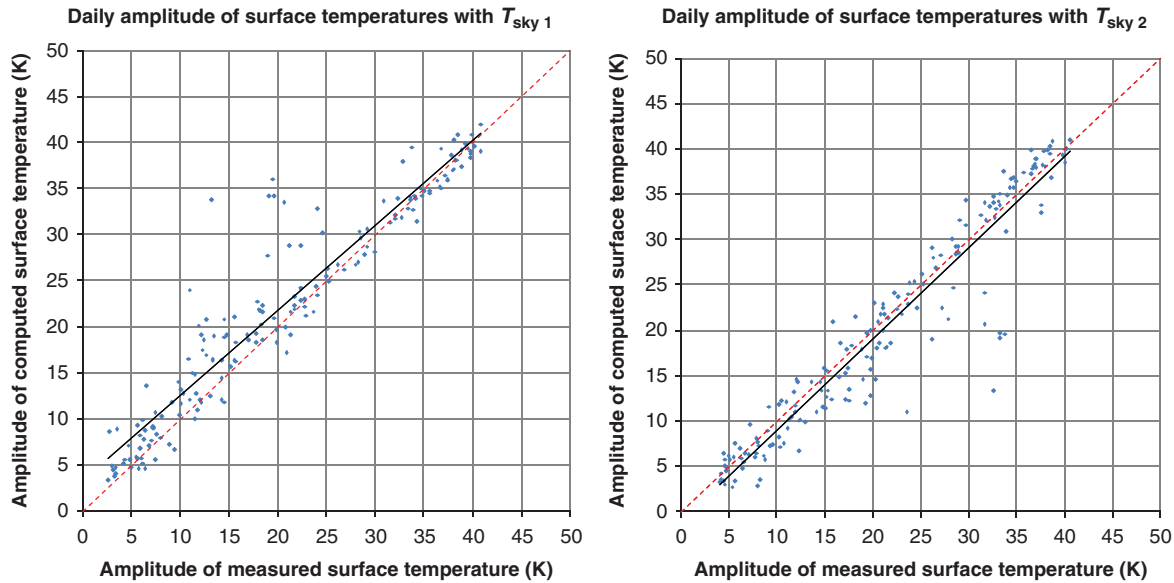
Figure 17. Daily variation of surface temperature, numerical versus experimental comparison (10 July 2012 to 31 December 2012).

This study enables us to identify this coefficient by inverse analysis in the future because of the sensitivity of this parameter. To access to such method, we need some temperature in each layers of the pavement.

4.4 *Surface temperature statistical results*

Now, we have to evaluate the thermal modelling over a longer period such as one year in order to lead to thermo-mechanical damage assessment. We can look at a one-year simulation in Figure 14 and comment the daily maximum and minimum surface temperatures which will be further introduced in a damage model. In this simulation, reference data are introduced as input (i.e. solar radiation, sky temperature as $T_{\text{sky 2}}$ formula, wind as variable convection coefficient and material properties such as those introduced in Table 1). We can see in Figure 15 that the model leads to a progressive deviation for both maximum and minimum daily temperatures, which become slightly overestimated compared with the measure. This phenomenon is not significant in the first part of the period (summer and autumn), as shown by the trend curve in Figure 15. However, this deviation increased more significantly during spring 2013. We can explain these differences by the very variable weather of the first semester in 2013, characterised by alternative strong periods of rain, wind and sun. It seems, in particular, that the succession of sun and rain showers strongly affects surface temperature. According to this, the positive deviation encountered in our model can be explained because the latent heat withdrawn for evaporation is not taken into account. The global deviation trend is stronger for daily maxima because the model does not assume the

frequent showers occurring during sunny days. During the night, the influence of water is less important, because evaporation is lower. The global deviation can be considered as a superposition of two phenomena: a cumulative massive deviation resulting from a systematic overestimation of surface temperature during rainy days, which is also visible in deeper layers, and also a statistical effect of many variable days which lead to a strong overestimation of the daily maximum.

The influence on the surface temperature of the chosen T_{sky} formula for LWL radiation is shown in Figures 16 and 17. As shown in the short-time study, $T_{\text{sky 1}}$ is statistically correct for the daily maximum evaluation, whilst it overstates daily minima. $T_{\text{sky 2}}$, which takes cloud covering into account, presents similar patterns between night and day (minimum and maximum, respectively). The resultant statistical result in terms of daily amplitude shows the best correlation between computation and measure. Thus, formula $T_{\text{sky 2}}$ is well suited to temperature field computations in the framework of long-term fatigue modelling.

5. Conclusion

In this study, we have presented the validation of a numerical model in a transient thermal calculation for a pavement surface subjected to variable weather conditions, including the effect of night-time cooling especially when the sky is clear. Assuming good night-time cooling (with LWL radiation) is absolutely necessary for a good assessment of daily temperature variation leading to thermal fatigue damage in the pavement. The various comparisons drawn demonstrate the significant

impact of night-time cooling on a refined temperature characterisation.

The comparison of numerical results, assuming long-wave radiation (night-time cooling), with experimental results enables us to validate the numerical model (mainly in the transient thermal calculation). The sensitivity analysis of this model has shown a significant impact of different parameters (heat transfer coefficient and thermal conductivity of layers); however, the effect of absorption coefficient and thermal inertia is low. This outcome is critical to further studies focusing on the thermo-mechanical behaviour of concrete pavement structures in hot dry zones. Let us remember that thermal cracking is caused by a daily temperature variation close to the surface layer, hence the importance of an accurate surface temperature variation evaluation. Actually, this climate modelling leads to a good approximation of temperature variation, inducing thermal cracking. For a better and further evaluation of absolute temperature, rain, shower, evaporation and icing effects have to be introduced in the model.

The main originality of this article is the beneficial effect of night-time cooling with the proposed long-wave radiation (LWL) modelling. For pavement design with thermal loading providing cracking, a significant contribution, in particular, during sky clear weather as in dry zones has been proposed here. However, other factors, such as humidity brought by showers or rainfall, were not considered in the present model. The uses of the sky formula enable the users to obtain a good modelling of the surface temperature. The uses of the sky formula in the model give a good correlation between the numerical and experimental results of the surface temperature daily variation. In pursuit of a refined model of surface temperature, other perspectives on thermal property identification of layers, by means of inverse methods, become accessible from temperature measurements inside the multilayered pavement.

References

Al-Abdul Wahhab, H.I. and Ramadhan, R.H., 1995. Manifestation of temperature variation of flexible and rigid pavement in Dhahran, Saudi Arabia. *The 4th Saudi engineering conference*, Vol. 2, November 1995.

Al-Abdul Wahhab, H.I. and Balghunaim, F., 1994. Asphalt pavement temperature related to arid Saudi environment. *Journal of Material in Civil Engineering*, 6 (1), 1–14.

Bissada, F., 1972. *Asphalt pavement temperature related to Kuwait climate*. Washington, DC: Transportation Research Board, Highway Research Record 404, 71–85.

Dempsy, B.J., Herlach, W.A., and Patel, A.J., 1985. *The climatic-material-structural pavement analysis program*, final report in FHWA/RD-84/113. Washington, DC: Federal Highway Administration.

El Ayadi, A., *et al.*, 2012. An improved dynamic model for the study of a flexible pavement. *Advances in Engineering Software*, 44, 44–53.

Hall, M.R., *et al.*, 2012. Influence of the thermophysical properties of pavement materials on the evolution of temperature depth profiles in different climatic regions. *Journal of Materials in Civil Engineering*, 24 (1), 32–47.

Hermansson, A., 2000. Simulation model for calculating pavement temperatures including maximum temperature. *Transportation Research Record* (1699), 134–141.

Hermansson, A., 2004. Mechanical model for paved surface summer and winter temperature: comparison of calculated and measured temperatures. *Cold Regions Science and Technology*, 40, 1–17.

Jensen, O.M. and Hansen, P.F., 1999. Influence of temperature on autogenous deformation and relative humidity change in hardening cement paste. *Cement and Concrete Research*, 29 (4), 567–575.

Jia, L., *et al.*, 2007. Numerical prediction model for asphalt concrete pavement. *Journal of Tongji University*, 35 (8), 1039–1043.

Laveissiere, D. and Petit, C., 1998. Modeling of fatigue cracking in precracked pavements under thermal stress. *Revue Générale des Routes*, 760, 49–53.

Lui, C. and Yuan, D., 2000. Temperature distribution in layered road structures. *Journal of Transportation Engineering*, 126 (1), 93–95.

Marcel, L., *et al.*, 2003. Design tool for thermal energy potential of asphalt pavements. *8th international IBPSA conference*. Eindhoven, Netherlands. August 11–14, 2003.

Martin, M. and Berdahl, P., 1984. Characteristics of infrared sky radiation in the United States. *Solar Energy*, 33 (3/4), 321–336.

Minhoto, M.J.C., Pais, J.C., and Pereira, P.A.A., 2006. Asphalt pavement temperature prediction. *Proceeding asphalt rubber 2006*. P194-207.

Nguyen, Q.T., 2011. *Thermomechanical behaviour of asphalt under cyclic loading in the linear and non-linear areas*. Thesis (PhD).

Nguyen, Q.T., Di Benedetto, H., and Sauzéat, C., 2012. Determination of thermal properties of asphalt mixtures as another output from cyclic tension-compression test. *Road Materials and Pavement Design*, 13 (1), 85–103.

Ramadhan, R.H. and Al-Abdul Wahhab, H.I., 1997. Temperature variation of flexible and rigid pavement in Eastern Saudi Arabia. *Building and Environment*, 32 (4), 367–373.

Solaimanian, M. and Kennedy, T.W., 1993. Prediction maximum pavement surface temperature using maximum air temperature and hourly solar radiation. *Transportation Research Record: Journal of Transportation Research Board*, 1417, 1–11.

Tao, F. and Shide, F., 2012. A Numerical model for predicting road surface temperature in the highway. *Procedia Engineering*, 37, 137–142.

Tzu-Ping, L., Yu-Feng, H., and Yu-Sung, H., 2007. Seasonal effect of pavement on outdoor thermal environment in subtropical Taiwan. *Building and Environment*, 42, 4124–4131.

Vautrin, S. and Livet, J., 1996. Winter operations pavement. Document Regional of Nancy Laboratory (France), June, p. 12.

Wang, D., Roesler, R.J., and Guo, D.Z., 2009. Analytical approach to predicting temperature fields in multilayered pavement systems. *Journal of Engineering Mechanics*, 135 (4), 334–344.

Yinghong, Q. and Hiller, J.E., 2011. Modeling temperature distribution in rigid pavement slabs: impact of air temperature. *Construction and Building Materials*, 25, 3753–3761.